Composite Structures 241 (2020) 112133

Contents lists available at ScienceDirect

Composite Structures

journal homepage: www.elsevier.com/locate/compstruct

The effect of plate theories and boundary conditions on the bending behavior of a biaxial corrugated core sandwich panel

Mostafa Mohammadabadi[a], Vikram Yadama[b,*], Lloyd Smith[c]

[a] Material Science and Engineering Program and Composite Materials and Engineering Center, Washington State University, Pullman, WA 99164, USA
[b] Department of Civil and Environmental Engineering and Composite Materials and Engineering Center, Washington State University, Pullman, WA 99164, USA
[c] School of Mechanical and Materials Engineering, Washington State University, Pullman, WA 99164, USA

ARTICLE INFO

Keywords:
Sandwich panel
Wood composite
Biaxial corrugated core
Effective properties
Generalized differential quadrature (GDQ) method
Homogenization method

ABSTRACT

In this study, an analytical model was developed to evaluate the bending behavior of a wood composite sandwich panel with a biaxial corrugated core. To explore the effect of shear deformation, two plate theories were considered: classical plate theory (CPT) and a third-order shear deformation plate theory (TOSDPT). The effect of simply supported-simply supported, clamped–clamped, and simply supported-free boundary conditions on the bending behavior of the sandwich panel was investigated. A homogenization method was used to replace the corrugated geometry of the core with a continuous layer. Based on the deformation of the corrugated core, the effective properties of the homogenized layer were obtained. Classical lamination theory and the principle of minimum potential energy were applied to derive the governing equations and apply the boundary conditions. A generalized differential quadrature method was applied to solve the governing differential equations. The bending stiffness of a panel with simply supported-free boundary conditions agreed with the experiment within 3.67% and 0.28% for CPT and TOSDPT, respectively.

1. Introduction

Bio-based sandwich structures that are environmentally friendly, renewable, and recyclable have been developed recently [1–5]. However, those with hollow cores have attracted interest because the hollow geometry of the core can be used to improve the thermal and acoustic performance.

Using the elastic constants developed by Libove and Hubka [6] for corrugated core sandwich panels, Chang et al. [7] employed a first-order shear deformation theory to understand the bending behavior of a uniaxial corrugated core sandwich panel with simply supported-simply supported (SSSS) and clamped–clamped (CCCC) boundary conditions. By computing the second moment of inertia for the sinusoidal cross section of a uniaxial corrugated core, Magnucki et al. [8] found the bending stiffness of a sandwich structure and evaluated the bending and buckling behavior. However, the effect of shear deformation was not included. Aboura el al. developed an analytical model to find the effective material properties of corrugated cardboard [9]. Considering the sinusoidal cross section of the uniaxial corrugated core, the global stiffness matrices were calculated for the cardboard. However, only the extensional stiffness matrix was used to obtain the effective properties. Cheon and Kim [10] suggested an equivalent plate model for uniaxial corrugated core sandwich panels with trapezoidal and sinusoidal corrugation. Using the equivalent energy method and classical plate theory, which does not take shear deformation into account, the extensional stiffness matrix and bending stiffness matrix were obtained to compute the effective material properties and thickness of a homogeneous plate. A finite element (FE) model of the actual geometry was used to verify the analytical model.

When the core geometry of a sandwich panel can be described by a known function, analytical models often allow relatively simple evaluation of the sandwich structure. However, the geometry of many panel cores are complex, i.e. a core where the geometry varies along both the length and width of the panel. Analytical models for these cases have found limited application.

Other researchers used the internal forces and deformations of the core to evaluate corrugated core sandwich panels. Using curved beam theory, Nordstand et al. [11] established the relation between applied loads and moments with displacements and rotations for a sinusoidal corrugated core sandwich panel. Effective transverse shear moduli, G_{xz} and G_{yz}, were obtained and compared with FE results and those obtained by Libove and Hubka [6]. Considering the deformation of a uniaxial corrugated core subjected to a unit displacement, Kazemahvazi and Zenkert [12] derived the relation between internal forces and

* Corresponding author.
E-mail address: vyadama@wsu.edu (V. Yadama).

https://doi.org/10.1016/j.compstruct.2020.112133
Received 3 November 2019; Received in revised form 22 February 2020; Accepted 24 February 2020
Available online 28 February 2020

Fig. 1. Biaxial corrugated wood composite core and corresponding sandwich panel.

global displacements to obtain the shear modulus, G_{xz}, and out-of-plane modulus, E_{zz}. A strength model that predicts the shear and normal stresses acting on the core members was developed and validated using the results obtained from FE. Bartolozzi et al. [13] found displacements caused by unit forces using Castigliano's theorem, and derived the material properties required for a first-order shear deformation theory. The bending stiffness and acoustic behavior of a sandwich panel with a uniaxial sinusoidal corrugated core were evaluated and compared with FE. Other approaches used to model and evaluate sandwich structures can be found in the review articles by Noor et al. [14] and Hohe and Becker [15]. To evaluate the bending behavior of sandwich beams with a biaxial corrugated core geometry, a high-order sandwich panel theory (HSAPT) was used [16] (Fig. 1). Based on the deformation and internal forces generated in a corrugated core subjected to a unit displacement, the effective properties were found. However, since beam theory was used, all deformation in the width direction was neglected, and the boundary conditions were defined only on opposing ends of the panels.

No analytical model has been developed for a full size sandwich panel with a biaxial corrugated core (shown in Fig. 1), where deformation in the width direction is considered, and boundary conditions can be defined on all four edges of the panel. Since this sandwich panel was developed as a construction material for building envelopes [5,17–19], development of an analytical model to evaluate a full size panel will help analyze the influence of geometry, reduce experimental work, and assist in designing new cores for targeted applications or specifications.

2. Materials

Thin wood strands with an average thickness of 0.36 mm were dried to a target moisture content of 3–5% and sprayed with aerosolized liquid phenol formaldehyde (PF) resin to a target resin content of 8% by oven-dry wood weight. Resinated wood strands were oriented and hand-formed unidirectionally (parallel to the *x*-axis shown in Fig. 2) to fabricate a wood strand mat or *preform*. The unidirectional mat was then consolidated in a hot press for 6 min into a corrugated core panel with a matched-die mold, or a flat panel without a mold for facesheets. To fabricate the sandwich panels, 6.35 mm thick flat panels were bonded with a polyurethane adhesive (LOCTITE HB X452 PURBOND, Henkel) to a biaxial corrugated core (Fig. 1) at room temperature. A unit cell (UC) of the biaxial corrugated core and its dimensions are shown in Fig. 2.

Because of the changing fiber direction in the core, a local coordinate system (1–2-3, where 1is parallel to the wood fibers and 2 is in plane and perpendicular to 1) was defined on each face of the core (Fig. 2b). Faces with the same color in Fig. 2b share the same local coordinate system. The local coordinate system on the facesheets is aligned with the global coordinate system. The elastic constants in the local coordinate system for both facesheets and the corrugated core [16] are given in Table 1.

3. Analytical model

In developing the analytical model, a homogenization method [15] was used to find the effective properties of the homogenous layer. Classical plate theory (CPT) and third-order shear deformation theory (TOSDPT) which have been used by many researchers for layered structures [6–9,16,20–30] and were used here to develop the analytical model and consider the effect of shear deformation. The displacement field for these theories in the global coordinate system (*x*, *y*, and *z*) can be defined as [31]

$$u_x = u_0(x,y) + z\phi_x(x,y) - c_1 z^3\left(\phi_x + \frac{\partial w_0}{\partial x}\right)$$
$$u_y = v_0(x,y) + z\phi_y(x,y) - c_1 z^3\left(\phi_y + \frac{\partial w_0}{\partial y}\right)$$
$$u_z = w_0(x,y) \quad (1)$$

where u_0, v_0 and w_0 are, respectively, the x-, y-, and z-components of the displacement at any point on the mid-plane of the panel, and ϕ_x and ϕ_y are the angle of rotation of the cross section about the y-axis and x-axis with respect to the z-axis, respectively. The panel geometry was

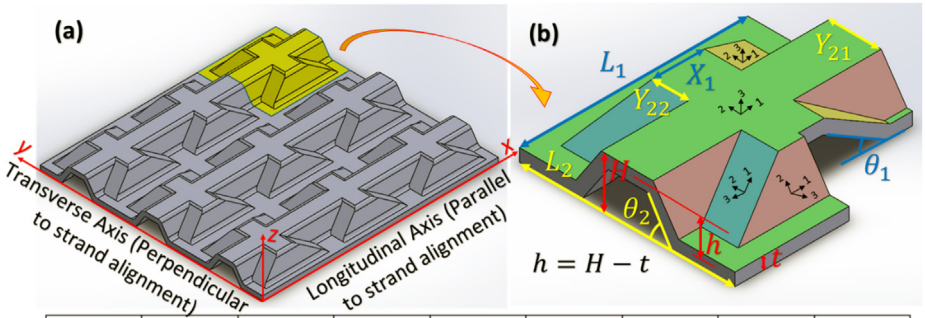

H	t	L_1	L_2	θ_1	θ_2	X_1	Y_{21}	Y_{22}
35	7.6	203	203	40	56	63	30	48

Fig. 2. Biaxial corrugated core (a) global coordinate system along with longitudinal and transverse directions (b) unit cell along with its dimensions and local coordinate system (dimensions are in mm).

Table 1
Elastic constants of wood composite material.

E_1(GPa)	E_2(GPa)	E_3(GPa)	υ_{12}	υ_{13}	υ_{23}	G_{12}(GPa)	G_{13} (GPa)	G_{23} (GPa)
9.80	1.71	1.71	0.358	0.358	0.2	2.56	2.56	0.71

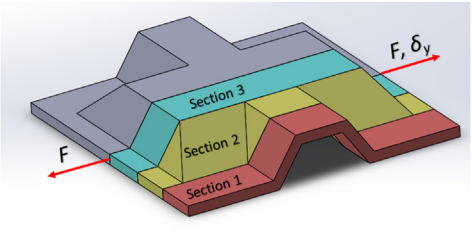

Fig. 3. UC under tensile loading to obtain the effective E_2.

described using$c_1 = 4\alpha/3H_t^2$, and $H_t = h_b + H + h_t$ where H_t and H are the height of the sandwich panel and core, respectively, and h_b and h_t are the thickness of the bottom and top facesheets, respectively, as shown in Fig. 2. Note when $\alpha = 1$ we have a third-order shear deformation plate theory, and when $\alpha = 0$, $\phi_x = -\partial w_0/\partial x$, and $\phi_y = -\partial w_0/\partial y$, so that the displacement field for classical plate theory is achieved.

3.1. Governing equations

The first variation of strain energy in a deformed material occupying region Ω is given by [32]

$$\delta U = \int_\Omega (\sigma_{ij}\delta\varepsilon_{ij})dv, \quad i,j = \mathrm{x, y, z} \tag{2}$$

where σ and ε are stress and strain tensors, respectively. The components of the strain tensor are

$$\varepsilon_{ij} = \frac{1}{2}(\nabla u + (\nabla u)^T) = \frac{1}{2}(u_{i,j} + u_{j,i}) = \varepsilon_{ji} \tag{3}$$

The components of displacement field (u_x, u_y andu_z) of any point of the panel in the coordinate system (x, y, and z) are given in Eq. (1). The constitutive relation to find the stresses can be defined as

$$\begin{bmatrix} \sigma_{xx}^{t,c,b} \\ \sigma_{yy}^{t,c,b} \\ \sigma_{zz}^{t,c,b} \\ \sigma_{yz}^{t,c,b} \\ \sigma_{xz}^{t,c,b} \\ \sigma_{xy}^{t,c,b} \end{bmatrix} = \begin{bmatrix} C_{11} & C_{12} & C_{13} & 0 & 0 & 0 \\ C_{12} & C_{22} & C_{23} & 0 & 0 & 0 \\ C_{13} & C_{23} & C_{33} & 0 & 0 & 0 \\ 0 & 0 & 0 & C_{44} & 0 & 0 \\ 0 & 0 & 0 & 0 & C_{55} & 0 \\ 0 & 0 & 0 & 0 & 0 & C_{66} \end{bmatrix}^{t,c,b} \begin{bmatrix} \varepsilon_{xx} \\ \varepsilon_{yy} \\ \varepsilon_{zz} \\ \gamma_{yz} \\ \gamma_{xz} \\ \gamma_{xy} \end{bmatrix} \tag{4}$$

where t and b indicate top and bottom facesheets, respectively, and c refers to the core. The components of stiffness matrix, C_{ij}, can be found in the literature [28]. The Poisson effect was not considered. The general form of the first variation of work done by the external forces is given by

$$\delta W = \int_\Omega [f_u\delta u_0 + f_v\delta v_0 + f_w\delta w_0]dxdy + \int_{\partial\Omega} [\bar{N}_{nx}\delta u_0 + \bar{N}_{ny}\delta v_0 + \bar{V}\delta w_0 + \bar{M}_n\delta\phi_n]ds \tag{5}$$

where f_u, f_v and f_w are, respectively, the x-, y- and z-components of the body force per unit length, and $\bar{N}_{nx}$ and$\bar{N}_{ny}$ are the axial forces, $\bar{V}$ and $\bar{M}_n$ are transverse force and bending moment at the boundary of the panel, respectively.

The governing equations can be derived using the principle of minimum potential energy as [33]

$$\delta\Pi = \delta U - \delta W = 0 \tag{6}$$

The governing equations are lengthy, and therefore, included in the Appendix.

4. Homogenization method

To introduce the core geometry into the analytical model, a homogenization method was used to replace the biaxial corrugated core with a continuous layer. The effective properties of an equivalent beam were derived from the internal forces and deformation caused by a unit displacement applied to a UC [16]. The remaining effective properties of the homogenized core were derived using linear beam theory as

$$\delta_T = \frac{F_T L}{AE}, \quad \delta_C = \frac{F_C L}{AE}, \quad \delta_S = \frac{F_S L}{GA}, \quad \delta_B = \frac{F_B L^3}{3EI} \tag{7}$$

where F and δ are the load and displacement, E and G are material properties, and A and I are area and moment of inertia of the beam. Tensile, compressive, shear and bending loads and corresponding displacements are denoted by subscripts T, C, S, and B, respectively.

4.1. Effective Young's modulus in the y-Direction, E_y^{eff}

Taking advantage of the geometric symmetry in the UC, the tensile deformation of one half of a UC (Fig. 3) was investigated. This half was divided into three sections. A thin element with a width of dx from each section was used to consider the load from a unit displacement. The cross sectional area and moment of inertia for different parts of the thin elements are shown in Fig. 4 and given in Table 2.

The height of the centroid line was used to compute the moment caused by an eccentric load, dF_i, as

$$h_i'' = \frac{2L_{ei}A_{ei}(h_i'/2) + L_{fi}A_{fi}(h_i')}{2L_{di}A_{di} + 2L_{ei}A_{ei} + L_{fi}A_{fi}} \quad i = 1, 3 \tag{8}$$

$$h_2'' = \frac{2L_kA_k\left(\frac{h'}{2}\right) + 2L_mA_m(h') + 2L_nA_n\left(\frac{h+h'}{2}\right) + L_pA_p(h)}{2L_gA_g + 2L_kA_k + 2L_mA_m + 2L_nA_n + L_pA_p}$$

Using Eqs. (7) and geometric parameters in Table 2, the load that acts on each element of width dx can be found in terms of a unit displacement δ_y as

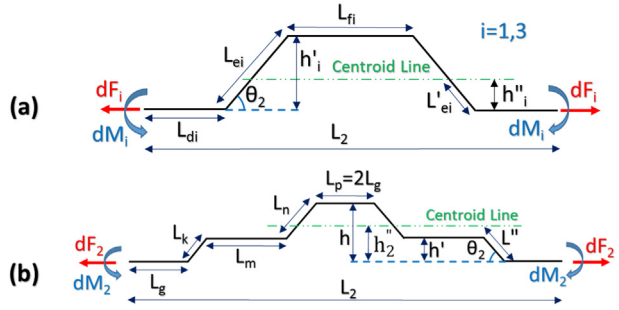

Fig. 4. Schematic view of thin elements cut from (a) sections 1 and 3 (b) Section 2 shown in Fig. 3. Subscripts d-p refer to straight element segments, corresponding to the definitions in Table 2. The subscript i refers to the section number, defined in Fig. 3, and the corresponding definitions in Table 2.

Table 2
Geometrical parameters specified in Fig. 4 for Sections 1–3.

Section	Geometric parameters shown in Fig. 4
1	$L_{d1} = Y_{22} + \frac{Y_{21}}{2}$, $L_{e1} = \frac{h_1^{'}}{sin\theta_2}$, $L_{f1} = Y_{21}$, $h_1^{'} = h$
	$A_{d1} = A_{e1} = A_{f1} = tdx$, $I_{e1} = \frac{t^3}{12}dx$, $x \in [0,\ X_1/2]$
2	$L_g = \frac{Y_{21}}{2}$, $L_k = \frac{h^{'}}{sin\theta_2}$, $L_m = Y_{22}$, $L_n = \frac{h-h^{'}}{sin\theta_2}$, $L_p = Y_{21}$, $h^{'} = x.\ tan\theta_1$
	$A_g = A_k = A_n = A_p = tdx$, $A_m = \frac{tdx}{cos\theta_1}$, $I_k = I_n = \frac{t^3dx}{12}$, $x \in [0,\ h/tan\theta_1]$
3	$L_{d3} = \frac{Y_{21}}{2}$, $L_{e3} = \frac{h_3^{'}}{sin\theta_2}$, $L_{f3} = 2Y_{22} + Y_{21}$, $h_3^{'} = h$
	$A_{d3} = A_{e3} = A_{f3} = tdx$, $I_{e3} = \frac{t^3}{12}dx$, $x \in [0,\ X_1/2]$

$$dF_i = \frac{\delta_y}{\left(\frac{2L_{di}}{A_{di}E_2} + \frac{2(sin\theta_2)^2(L_{ei}^{'3} + (L_{ei} - L_{ei}^{'})^3)}{3E_2I_{ei}} + \frac{2(sin\theta_2)^2L_{ei}}{G_{23}A_{ei}} + \frac{2(cos\theta_2)^2L_{ei}}{A_{ei}E_2} + \frac{L_{fi}}{A_{fi}E_2}\right)}$$

$i = 1, 3$

$$dF_2 = \frac{\delta_y}{\left(\begin{array}{l}\frac{2L_g}{A_gE_2} + \frac{2L_m}{A_mE_2} + \frac{2(L_p/2)}{A_p.E_2} + \frac{2(L^{''} - L_k)(sin\theta_2)^2L_k^2}{2E_2I_k} \\ + \frac{2(sin\theta_2)^2(L_n + L_k)}{G_{23}A_n} \\ + \frac{2(sin\theta_2)^2[(L_n + L_k - L^{''})^3 + (L^{''} - L_k)^3 + L_k^3]}{3E_2I_n} + \frac{2(cos\theta_2)^2(L_n + L_k)}{A_nE_2}\end{array}\right)} x$$

$\in [0,\ 0.5h/tan\theta_1]$

$$dF_2 = \frac{\delta_y}{\left(\begin{array}{l}\frac{2L_g}{A_gE_2} + \frac{2L_m}{A_mE_2} + \frac{2(L_p/2)}{A_pE_2} + \frac{2(sin\theta_2)^2[(L^{''})^3 + (L_k - L^{''})^3 + L_{\tilde{n}}^3]}{3E_2I_k} + \\ \frac{2(sin\theta_2)^2(L_k + L_n)}{G_{23}A_k} + \frac{2(cos\theta_2)^2(L_k + L_n)}{A_kE_2} + \frac{2(L_k - L^{''})(sin\theta_2)^2L_{\tilde{n}}^2}{2E_2I_n}\end{array}\right)} x$$

$\in [0.5h/tan\theta_1,\ h/tan\theta_1]$ $_i$ (9)

The tensile load for sections 1, 2, and 3 was computed by integrating dF_i over the width of the corresponding section. The effective longitudinal Young's modulus of the core was found from

$$E_y^{eff} = \frac{2L_2(F_1 + F_2 + F_3)}{HL_1}\delta_y \quad (10)$$

4.2. Effective shear modulus in the y-z Plane, G_{yz}^{eff}

Since the geometry of the core is complex and includes parts with varying cross section through the height of the UC, it is difficult to derive an effective shear modulus using the internal forces and deformation. Therefore, finite element analysis was used to find an equivalent and simplified geometry that represented the shear behavior of the actual geometry. The shear deformation of this simplified geometry was used to find the effective shear modulus. An actual UC under shear in the y-z plane is shown in Fig. 5a; whereas, a simplified UC, with similar shear behavior is shown in Fig. 5b. The UC was simplified by moving the outer walls (green) inward, forming a continuous inward wall (green). The shear modulus, G_{yz}, of the simplified geometry was 2.35% lower than the actual geometry. When a simplified UC (Fig. 5b) is subjected to a shear displacement, the red sections undergo shear deformation as shown in Fig. 6a, while the green sections experience tension/compression, shear, and bending deformation as shown in Fig. 6b.

The load caused by a unit displacement (δ_{yz}) in the red sections shown in Fig. 6a is

$$F_1 = \frac{2G_{12}t_MY_{22}}{H^{''}}\delta_{yz} \quad (11)$$

For the green sections shown in Fig. 6b, the load can be expressed in terms of a unit displacement as

$$F_2 = \frac{\delta_{yz}}{\left[\frac{4(\sin\theta_2)^2.H^{'3}}{E_2L_2t^3} + \frac{(\sin\theta_2)^2H^{'}}{G_{23}L_2t} + \frac{(\cos\theta_2)^2.H^{'}}{E_2L_2t}\right]} \quad (12)$$

The effective shear modulus in the *y-z* plane can then be written as

$$G_{yz}^{eff} = \frac{2H(F_1 + F_2)}{L_1L_2\delta_{yz}} = \frac{H}{L_1L_2}\left(\frac{2}{\left[\frac{4(\sin\theta_2)^2.H^{'3}}{E_2L_2t^3} + \frac{(\sin\theta_2)^2H^{'}}{G_{23}L_2t} + \frac{(\cos\theta_2)^2.H^{'}}{E_2L_2t}\right]} + \frac{4G_{12}t_MY_{22}}{H^{''}}\right) \quad (13)$$

4.3. Effective shear modulus in the x-y Plane, G_{xy}^{eff}

Finite element analysis was also used to find a simplified geometry that has the same shear behavior as the actual geometry under a unit displacement ofδ_{xy}. Both the actual and simplified geometries are shown in Fig. 7. The shear modulus in the *x-y* plane (G_{xy}) of the simplified geometry was 0.66% higher than the actual geometry.

To evaluate the shear behavior of the UC, the simplified geometry was divided into four sections as shown in Fig. 7b. The load generated by a unit displacement δ_{xy} in each of the sections is

$$F_1 = \frac{G_{12}t\left(\frac{Y_{21}}{2} + \frac{H}{\tan(\theta_2)} - \frac{t}{\sin(\theta_2)}\right)}{L_1}\delta_{xy} \quad (14a)$$

$$F_2 = \frac{H}{sin\theta_2\left[\frac{4}{E_1}\left(\frac{L_1}{t}\right)^3 + \frac{1}{G_{13}}\left(\frac{L_1}{t}\right)\right]}\delta_{xy} \quad (14b)$$

$$F_3 = \frac{G_{12}t(Y_{22} - \frac{t}{\sin(\theta_2)})}{L_1 + 2\left(\frac{H}{\sin(\theta_2)} - t\right)}\delta_{xy} \quad (14c)$$

$$F_4 = \frac{G_{12}t\left(\frac{L_2}{2} + \frac{2t}{\sin(\theta_2)} - \frac{Y_{21}}{2} - Y_{22} - t - \frac{H}{\tan(\theta_2)}\right)}{L_1}\delta_{xy} \quad (14d)$$

Using the loads for each section given in Eq. (14), the effective shear modulus in the *x-y* plane is

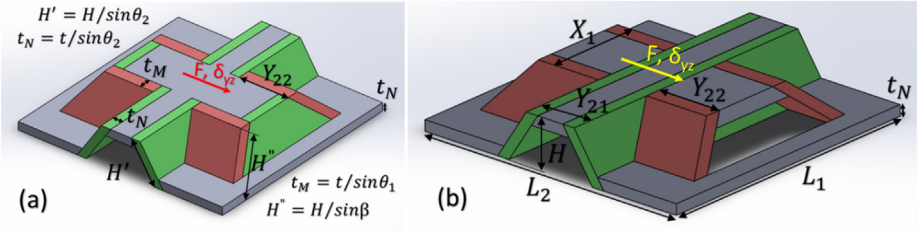

Fig. 5. A UC of the corrugated core (a) actual geometry (b) simplified geometry, with similar shear behavior in the y-z plane.

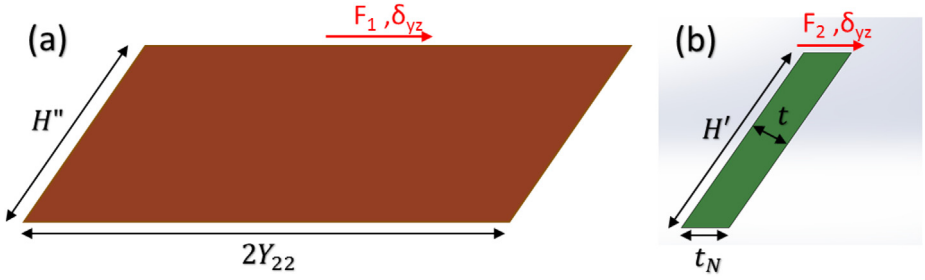

Fig. 6. Generated load in different parts of the UC with the simplified geometry shown in Fig. 5b.

$$G_{xy}^{eff} = \frac{2L_1(F_1+F_2+F_3+F_4)}{H'L_2\delta_{xy}} = \frac{2L_1\sin(\theta_2)}{HL_2}\left(\frac{G_{12}t\left(\frac{L_2}{2}+\frac{t}{\sin(\theta_2)}-Y_{22}-t\right)}{L_1}+\frac{G_{12}t\left(Y_{22}-\frac{t}{\sin(\theta_2)}\right)}{\left[L_1+2\left(\frac{H}{\sin(\theta_2)}-t\right)\right]}+\frac{H}{sin\theta_2\left[\frac{4}{E_1}\left(\frac{L_1}{t}\right)^3+\frac{1}{G_{13}}\left(\frac{L_1}{t}\right)\right]}\right) \quad (15)$$

5. FE model

Abaqus finite element software (version 6.14-1) was used to simulate the bending behavior of the actual geometry of the panels under different loading and boundary conditions. The corrugated core was modeled using shell elements, while solid elements were used to model the facesheets. The nodes of the facesheets and 3-D core were tied together as occurs for ideal adhesion. The model was run in displacement control.

6. Experimental procedure

As shown in Fig. 8, three sandwich panels were tested in four-point bending with simple supports on opposing ends and free conditions on the remaining ends (SSFF). These experimental results were used to verify the analytical and FE models under the same boundary conditions.

7. GDQ method

The generalized differential quadrature (GDQ) method has been used by many researchers [34–38] to solve partial differential equations. Unlike the Fourier series expansion that are commonly used for simply supported boundary conditions, GDQ can be applied for fixed and free boundary conditions. The GDQ method discretizes the domain into several sample points which are non-uniformly spaced and are obtained from the following equations as

$$x_i = \frac{a}{2}\left(1-cos\left(\frac{(i-1)\pi}{N-1}\right)\right)\ i=1\cdots N$$
$$y_j = \frac{b}{2}\left(1-cos\left(\frac{(j-1)\pi}{M-1}\right)\right)\ j=1\cdots M \quad (16)$$

where N and M are the number of the grid points in the x and y direction, respectively. The derivatives of a function at the grid point (x_i, y_i) can be discretized as

$$f_x^{(n)}(x_i,y_j)=\sum_{k=1}^{N}A_{ik}^{(n)}f(x_k,y_j)$$
$$f_y^{(m)}(x_i,y_j)=\sum_{l=1}^{M}B_{jl}^{(m)}f(x_i,y_l)$$
$$f_{xy}^{(n+m)}(x_i,y_j)=\sum_{k=1}^{N}\sum_{l=1}^{M}A_{ik}^{(n)}B_{jl}^{(m)}f(x_k,y_l) \quad (17)$$

The weighting coefficients $A_{ik}^{(n)}$ and $B_{jl}^{(m)}$ can be found in the literature [39].

8. Results and discussions

Three sandwich panels with SSFF boundary conditions were tested in four-point bending (Fig. 9). Dimensions of the sandwich panels are given in Fig. 8. The experimental results of the bending test are presented in Fig. 9.

The average linear bending stiffness from three sandwich panels is compared with the analytical and FE results in Fig. 10. The bending stiffness from the FE model and classical plate theory were 4.7% and 3.7% higher than experiment, respectively, while the third-order shear deformation plate theory was 0.3% higher. Surprisingly, for a panel with a relatively large span, agreement with experiment improved when shear deformation was considered.

Since distributed loads (i.e. snow and wind) are common for construction materials, the bending behavior of the sandwich panels under a distributed load is of interest. Since experimental data was not available for this test, the plate theories were compared to the FE model. A uniform pressure of 34.5 kPa was applied over the surface of the panel for SSSS and CCCC boundary conditions. The slope of the load–deflection at the center of the panel, which is proportional to the bending stiffness, is compared in Fig. 11.

For SSSS, stiffness from CPT and TOSDPT exceeded the FE model by 3.3% and 1.3%, respectively. For CCCC, the stiffness from CPT and TOSDPT exceeded the FE model by 14.2% and 6.3%, respectively.

Both the facesheets and the core of the sandwich panel evaluated in

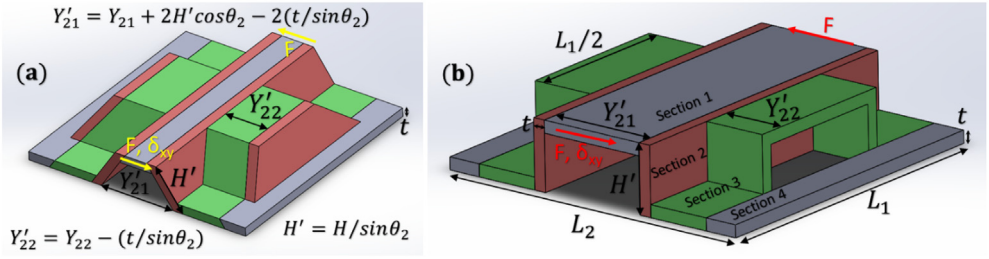

Fig. 7. A UC of the corrugated core (a) actual geometry (b) simplified geometry with similar shear behavior in the x-y plane.

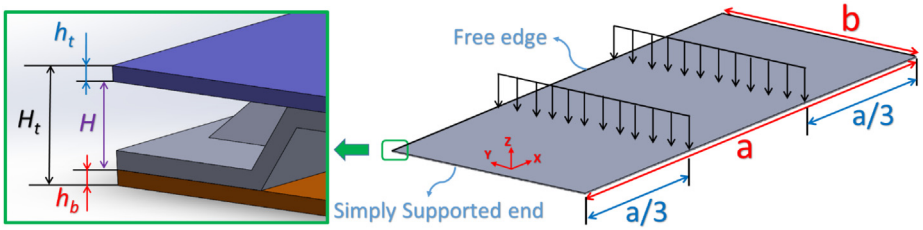

Fig. 8. Schematic view of a four-point bending experiment of a sandwich panel with simple supports. a = 2438 mm, b = 1219 mm, h_t = h_b = 6.35 mm, H = 35 mm.

this study were a wood composite. However, facesheets of a sandwich structure are often stiffer than the core. Fig. 12 shows the sensitivity of the stiffness of a SSSS panel with a uniform pressure on the change in the core and facesheet properties using TOSDPT.

The longitudinal and transverse modulus of the core (E_1^c, E_2^c) had a negligible effect on the bending stiffness of the sandwich panel. The longitudinal and transverse modulus of the facesheets (E_1^f, E_2^f) has a larger influence on the bending stiffness. DoublingE_1^f andE_2^f increased the bending stiffness of the sandwich panel by 11% and 32.8%, respectively. These results demonstrate the utility of predictive models in describing the responses of structural panels.

9. Limitations

The edge effect, which occurs when there is a mismatch in material properties of two adjacent layers along free edges, can affect the panel failure load [40–42]. Edge effects were neglected here since this study considered the linear behavior of sandwich panels. This approach was justified from an FE model, that considered edge effects, on a panel with SSFF boundary conditions. It was observed that the stresses associated with edge effects are at most 1.5% of the bending stresses. Edge effects also had a negligible effect on the distribution of bending stresses in the facesheets. While edge effects were negligible in this study, they should be considered for sandwich panels with different geometries and dimensions of that considered here.

10. Conclusions

An analytical model using two different plate theories was developed to evaluate the linear bending behavior of a sandwich panel with a biaxial corrugated core. A homogenization method was employed to replace the non-homogenous geometry with a continuous and homogenous layer. A GDQ method was used to solve the governing equations of the panels subjected to two different loadings, and three types of boundary conditions. For all loading and boundary conditions considered here, the TOSDPT model agreed better with experiment and numerical simulations than the CPT model. The results showed that shear deformation is important in these sandwich panels, even for cases involving relatively large span.

The analytical model was used in a parametric study that considered

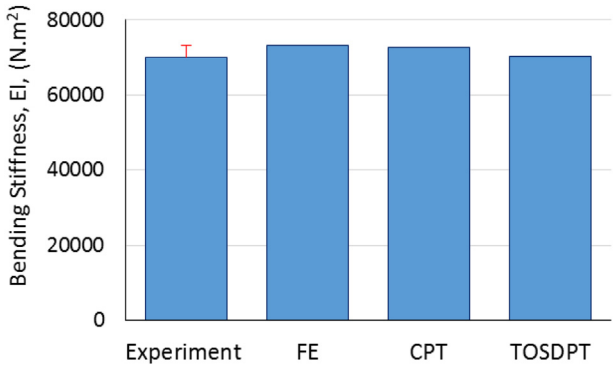

Fig. 10. Experimental, FE, and analytical bending stiffness of a sandwich panel subjected to four-point bending and SSFF boundary conditions. Error bar represents one standard deviation, or COV = 4.5%.

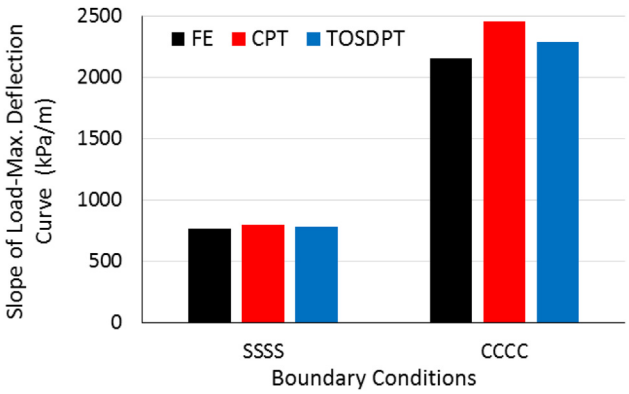

Fig. 11. Slope of the load–deflection curve of the panels subjected to a distributed load with SSSS and CCCC boundary conditions.

the effect of the properties of the core and facesheets on the bending stiffness of the panel. Increasing the modulus of the facesheets in both the longitudinal and transverse directions had a significant influence on the panel bending stiffness, while the effect of the core modulus was negligible. The results demonstrate the utility of using predictive

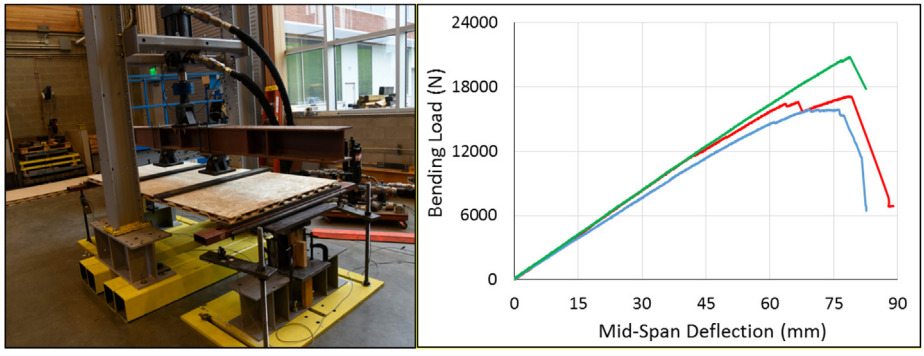

Fig. 9. Four-point bending test and load- mid-span deflection curves for sandwich panels with SSFF boundary conditions.

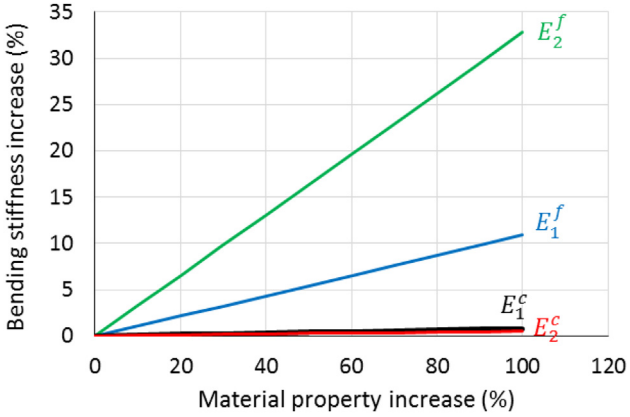

Fig. 12. The effect of the properties of the core and face sheet on the panel bending stiffness.

models to describe the response of structural panels.

CRediT authorship contribution statement

Mostafa Mohammadabadi: Methodology, Software, Validation, Formal analysis, Investigation, Writing - original draft, Visualization. **Vikram Yadama:** Conceptualization, Methodology, Formal analysis, Supervision, Project administration, Funding acquisition, Data curation, Writing - review & editing. **Smith Lloyd:** Formal analysis, Writing - review & editing.

Declaration of Competing Interest

The authors declare that they have no known competing financial interests or personal relationships that could have appeared to influence the work reported in this paper.

Acknowledgment

The authors would like to thank the National Science Foundation of USA, division CMMI for funding this research, grant # 1150316.

Data availability

The raw/processed data required to reproduce these findings cannot be shared at this time due to time limitations, however, data will be provided upon request.

Appendix

The governing equations in terms of displacement are expressed as

$$a_0\frac{\partial^2 u_0}{\partial x^2}+d_0\frac{\partial^2 u_0}{\partial y^2}+(b_0+d_0)\frac{\partial^2 v_0}{\partial x\partial y}+(a_1-c_1a_3)\frac{\partial^2\phi_x}{\partial x^2}+(d_1-c_1d_3)\frac{\partial^2\phi_x}{\partial y^2}+(b_1-c_1b_3+d_1-c_1d_3)\frac{\partial^2\phi_y}{\partial x\partial y}-c_1a_3\frac{\partial^3 w_0}{\partial x^3}+(-c_1b_3-2c_1d_3)\frac{\partial^3 w_0}{\partial x\partial y^2}+f_u=0. \tag{A.1}$$

$$e_0\frac{\partial^2 v_0}{\partial y^2}+d_0\frac{\partial^2 v_0}{\partial x^2}+(b_0+d_0)\frac{\partial^2 u_0}{\partial x\partial y}+(e_1-c_1e_3)\frac{\partial^2\phi_y}{\partial y^2}+(d_1-c_1d_3)\frac{\partial^2\phi_y}{\partial x^2}+(b_1-c_1b_3+d_1-c_1d_3)\frac{\partial^2\phi_x}{\partial x\partial y}-c_1e_3\frac{\partial^3 w_0}{\partial y^3}+(-c_1b_3-2c_1d_3)\frac{\partial^3 w_0}{\partial y\partial x^2}+f_v=0 \tag{A.2}$$

$$(a_1-c_1a_3)\frac{\partial^2 u_0}{\partial x^2}+(d_1-c_1d_3)\frac{\partial^2 u_0}{\partial y^2}+(b_1-c_1b_3+d_1-c_1d_3)\frac{\partial^2 v_0}{\partial x\partial y}+(a_2-2c_1a_4+c_1^2a_6)\frac{\partial^2\phi_x}{\partial x^2}+(d_2-2c_1d_4+c_1^2d_6)\frac{\partial^2\phi_x}{\partial y^2}+(-c_1a_4+c_1^2a_6)\frac{\partial^3 w_0}{\partial x^3}+(b_2-2c_1b_4+c_1^2b_6+d_2-2c_1d_4+c_1^2d_6)\frac{\partial^2\phi_y}{\partial x\partial y}+(-c_1b_4+c_1^2b_6-2c_1d_4+2c_1^2d_6)\frac{\partial^3 w_0}{\partial x\partial y^2}+(-f_0+2c_2f_2-c_2^2f_4)\left(\phi_x+\frac{\partial w_0}{\partial x}\right)=0 \tag{A.3}$$

$$(e_1-c_1e_3)\frac{\partial^2 v_0}{\partial y^2}+(d_1-c_1d_3)\frac{\partial^2 v_0}{\partial x^2}+(b_1-c_1b_3+d_1-c_1d_3)\frac{\partial^2 u_0}{\partial x\partial y}+(e_2-2c_1e_4+c_1^2e_6)\frac{\partial^2\phi_y}{\partial y^2}+(d_2-2c_1d_4+c_1^2d_6)\frac{\partial^2\phi_y}{\partial x^2}+(-c_1e_4+c_1^2e_6)\frac{\partial^3 w_0}{\partial y^3}+(b_2-2c_1b_4+c_1^2b_6+d_2-2c_1d_4+c_1^2d_6)\frac{\partial^2\phi_x}{\partial x\partial y}+(-c_1b_4+c_1^2b_6-2c_1d_4+2c_1^2d_6)\frac{\partial^3 w_0}{\partial y\partial x^2})+(-g_0+2c_2g_2-c_2^2g_4)\left(\phi_y+\frac{\partial w_0}{\partial y}\right)=0 \tag{A.4}$$

$$c_1a_3\frac{\partial^3 u_0}{\partial x^3}+c_1e_3\frac{\partial^3 v_0}{\partial y^3}+(c_1a_4-c_1^2a_6)\frac{\partial^3\phi_x}{\partial x^3}+(c_1e_4-c_1^2e_6)\frac{\partial^3\phi_y}{\partial y^3}+(2c_1d_3+c_1b_3)\frac{\partial^3 u_0}{\partial y^2\partial x}+(2c_1d_3+c_1b_3)\frac{\partial^3 v_0}{\partial x^2\partial y}+(c_1b_4-c_1^2b_6-2c_1^2d_6+2c_1d_4)\frac{\partial^3\phi_x}{\partial y^2\partial x}+(c_1b_4-c_1^2b_6-2c_1^2d_6+2c_1d_4)\frac{\partial^3\phi_y}{\partial x^2\partial y}-c_1^2a_6\frac{\partial^4 w}{\partial x^4}-c_1^2e_6\frac{\partial^4 w}{\partial y^4}+(-2c_1^2b_6-4c_1^2d_6)\frac{\partial^4 w}{\partial y^2\partial x^2}+(f_0-2c_2f_2+c_2^2f_4)\left(\frac{\partial^2 w}{\partial x^2}+\frac{\partial\phi_x}{\partial x}\right)+(g_0-2c_2g_2+c_2^2g_4)\left(\frac{\partial^2 w}{\partial y^2}+\frac{\partial\phi_y}{\partial y}\right)-\left(\bar{N}_{xx}\frac{\partial^2 w_0}{\partial x^2}+2\bar{N}_{xy}\frac{\partial^2 w_0}{\partial y\partial x}+\bar{N}_{yy}\frac{\partial^2 w_0}{\partial y^2}\right)+f_w=0 \tag{A.5}$$

where $c_2 = 3c_1$, and other coefficients are defined as

$$\begin{Bmatrix} a_0 \\ a_1 \\ a_2 \\ a_3 \\ a_4 \\ a_6 \end{Bmatrix} = \int_{-H_t/2}^{H_t/2} C_{11} \begin{Bmatrix} 1 \\ z \\ z^2 \\ z^3 \\ z^4 \\ z^6 \end{Bmatrix} dz, \quad \begin{Bmatrix} b_0 \\ b_1 \\ b_2 \\ b_3 \\ b_4 \\ b_6 \end{Bmatrix} = \int_{-H_t/2}^{H_t/2} C_{12} \begin{Bmatrix} 1 \\ z \\ z^2 \\ z^3 \\ z^4 \\ z^6 \end{Bmatrix} dz$$

$$\begin{Bmatrix} e_0 \\ e_1 \\ e_2 \\ e_3 \\ e_4 \\ e_6 \end{Bmatrix} = \int_{-H_t/2}^{H_t/2} C_{22} \begin{Bmatrix} 1 \\ z \\ z^2 \\ z^3 \\ z^4 \\ z^6 \end{Bmatrix} dz, \quad \begin{Bmatrix} d_0 \\ d_1 \\ d_2 \\ d_3 \\ d_4 \\ d_6 \end{Bmatrix} = \int_{-H_t/2}^{H_t/2} C_{66} \begin{Bmatrix} 1 \\ z \\ z^2 \\ z^3 \\ z^4 \\ z^6 \end{Bmatrix} dz$$

$$\begin{Bmatrix} f_0 \\ f_1 \\ f_2 \\ f_3 \\ f_4 \\ f_6 \end{Bmatrix} = \int_{-H_t/2}^{H_t/2} C_{55} \begin{Bmatrix} 1 \\ z \\ z^2 \\ z^3 \\ z^4 \\ z^6 \end{Bmatrix} dz, \quad \begin{Bmatrix} g_0 \\ g_1 \\ g_2 \\ g_3 \\ g_4 \\ g_6 \end{Bmatrix} = \int_{-H_t/2}^{H_t/2} C_{44} \begin{Bmatrix} 1 \\ z \\ z^2 \\ z^3 \\ z^4 \\ z^6 \end{Bmatrix} dz \tag{A.6}$$

Since all coefficients given in Eq. (A.6) with odd subscripts are zero, only Eqs. (A.3)–(A.5) must be solved to obtain the deflection of the sandwich panel.

References

[1] Banerjee S, Bhattacharyya D. Optimal design of sandwich panels made of wood veneer hollow cores. Compos Sci Technol 2011;71(4):425–32.
[2] Way Daniel, et al. Evaluation of a wood-strand molded core sandwich panel. J Mater Civ Eng 2016;28(9):04016074.
[3] Rao Sanjeev, Jayaraman Krishnan, Bhattacharyya Debes. Short fibre reinforced cores and their sandwich panels: Processing and evaluation. Compos A Appl Sci Manuf 2011;42(9):1236–46.
[4] McCracken Aidan, Sadeghian Pedram. Corrugated cardboard core sandwich beams with bio-based flax fiber composite skins. J Build Eng 2018;20:114–22.
[5] Voth Christopher, White Nathan, Yadama Vikram, Cofer William. Design and Evaluation Of Thin-Walled Hollow-Core Wood-Strand Sandwich Panels. J Renew Mater 2015;3(3):234–43. https://doi.org/10.7569/JRM.2015.634109.
[6] Libove, Charles, and Ralph E. Hubka. “Elastic constants for corrugated-core sandwich plates.” (1951).
[7] Chang Wan-Shu, et al. Bending behavior of corrugated-core sandwich plates. Compos Struct 2005;70(1):81–9.
[8] Magnucki Krzysztof, et al. Strength and buckling of sandwich beams with corrugated core. J Theoret Appl Mech 2013;51(1):15–24.
[9] Aboura Z, Talbi N, Allaoui S, Benzeggagh ML. Elastic behavior of corrugated cardboard: experiments and modeling. Compos Struct 2004;63(1):53–62. https://doi.org/10.1016/S0263-8223(03)00131-4.
[10] Cheon Young-Jo, Kim Hyun-Gyu. An equivalent plate model for corrugated-core sandwich panels. J Mech Sci Technol 2015;29(3):1217–23.
[11] Nordstrand Tomas, Carlsson Leif A, Allen Howard G. Transverse shear stiffness of structural core sandwich. Compos Struct 1994;27(3):317–29.
[12] Kazemahvazi Sohrab, Zenkert Dan. Corrugated all-composite sandwich structures. Part 1: Modeling. Compos Sci Technol 2009;69(7-8):913–9.
[13] Bartolozzi Giorgio, et al. An equivalent material formulation for sinusoidal corrugated cores of structural sandwich panels. Compos Struct 2013;100:173–85.
[14] Noor Ahmed K, Scott Burton W, Bert Charles W. Computational models for sandwich panels and shells. Appl Mech Rev 1996;49(3):155–99.
[15] Hohe Jorg, Becker Wilfried. Effective stress-strain relations for two-dimensional cellular sandwich cores: homogenization, material models, and properties. Appl Mech Rev 2002;55(1):61–87.
[16] Mohammadabadi Mostafa, Yadama Vikram, Lloyd Smith. An Analytical Model for Wood Composite Sandwich Beams with a Biaxial Corrugated Core under Bending. Compos Struct 2019;111316.
[17] Mohammadabadi Mostafa, Yadama Vikram, Geng Jian. Creep behavior of 3D core wood-strand sandwich panels. Holzforschung 2018;72(6):513–9.
[18] Mohammadabadi Mostafa, et al. Low-velocity impact response of wood-strand sandwich panels and their components. Holzforschung 2018;72(8):681–9.
[19] Mohammadabadi Mostafa, Yadama Vikram. Influence of a biaxially corrugated core geometry on flexural stiffness of wood-strand composite sandwich panels. Mater Today Commun 2020;23:100931. https://doi.org/10.1016/j.mtcomm.2020.100931.
[20] He Li, Cheng Yuan-Sheng, Liu Jun. Precise bending stress analysis of corrugated-core, honeycomb-core and X-core sandwich panels. Compos Struct 2012;94(5):1656–68.
[21] Carlsson Leif A, Kardomateas George A. Structural and failure mechanics of sandwich composites Vol. 121. Springer Science & Business Media; 2011.
[22] Rohwer Klaus, Friedrichs Stefan, Wehmeyer Christof. Analyzing laminated structures from fibre-reinforced composite material. Technische Mechanik Sci J Fundam Appl Eng Mech 2005;25(1):59–79.
[23] Sun CT, Chin H. Analysis of asymmetric composite laminates. AIAA J 1988;26(6):714–8.
[24] Whitney, JM., and NJ. Pagano. “Shear deformation in heterogeneous anisotropic plates.” (1970): 1031-1036.
[25] Dong S.B, F. K. W. Tso. “On a laminated orthotropic shell theory including transverse shear deformation.” (1972): 1091–1097.
[26] Reddy Junuthula N. A simple higher-order theory for laminated composite plates. J Appl Mech 1984;51(4):745–52.
[27] Phan ND, Reddy JN. Analysis of laminated composite plates using a higher-order shear deformation theory. Int J Numer Meth Eng 1985;21(12):2201–19.
[28] Jones Robert M. Mechanics of composite materials. CRC Press; 2014.
[29] Hyer Michael W, White Scott R. Stress analysis of fiber-reinforced composite materials. DEStech Publications Inc; 2009.
[30] Gibson Ronald F. Principles of composite material mechanics. CRC Press; 2016.
[31] Yongqiang Li, Dawei Zhu. Free flexural vibration analysis of symmetric rectangular honeycomb panels using the improved Reddy’s third-order plate theory. Compos Struct 2009;88(1):33–9.
[32] Wang CM Junuthula Narasimha Reddy, Lee KH, eds. Shear deformable beams and plates: Relationships with classical solutions. Elsevier, 2000.
[33] Mohammad-Abadi M, Daneshmehr AR. Size dependent buckling analysis of microbeams based on modified couple stress theory with high order theories and general boundary conditions. Int J Eng Sci 2014;74:1–14.
[34] Abediokhchi J, Shakouri M, Kouchakzadeh MA. Bending analysis of moderately thick functionally graded conical panels with various boundary conditions using GDQ method. Compos Struct 2013;103:68–74.
[35] Tornabene Francesco, Fantuzzi Nicholas, Bacciocchi Michele. The GDQ method for the free vibration analysis of arbitrarily shaped laminated composite shells using a NURBS-based isogeometric approach. Compos Struct 2016;154:190–218.
[36] Hong CC. GDQ analysis of a beam-plate with delaminations. Compos Struct 2017;182:237–41.
[37] Salehipour H, Shahsavar A, Civalek O. Free vibration and static deflection analysis of functionally graded and porous micro/nanoshells with clamped and simply supported edges. Compos Struct 2019;221:110842.
[38] Mohammad-Abadi M, Daneshmehr AR. Modified couple stress theory applied to dynamic analysis of composite laminated beams by considering different beam theories. Int J Eng Sci 2015;87:83–102.
[39] Kurtaran Hasan. Geometrically nonlinear transient analysis of moderately thick laminated composite shallow shells with generalized differential quadrature method. Compos Struct 2015;125:605–14.
[40] Herakovich Carl T. On the relationship between engineering properties and delamination of composite materials. J Compos Mater 1981;15(4):336–48.
[41] Herakovich CT. Edge effects and delamination failures. J Strain Anal Eng Design 1989;24(4):245–52.
[42] Mittelstedt Christian, Becker Wilfried. Free-edge effects in composite laminates. Appl Mech Rev 2007;60(5):217–45.